2017

Single-molecule visualization of Saccharomyces cerevisiae leading-strand synthesis reveals dynamic interaction between MTC and the replisome

Jacob S. Lewis
University of Wollongong, jacobl@uow.edu.au

Lisanne Spenkelink
University of Wollongong, *University of Groningen*, ls808@uowmail.edu.au

Grant D. Schauer
Rockefeller University

Flynn R. Hill
University of Wollongong, flynn@uow.edu.au

Roxanna E. Georgescu
Rockefeller University

See next page for additional authors

Publication Details

Lewis, J. S., Spenkelink, L. M., Schauer, G. D., Hill, F. R., Georgescu, R. E., O'Donnell, M. E. & van Oijen, A. M. (2017). Single-molecule visualization of Saccharomyces cerevisiae leading-strand synthesis reveals dynamic interaction between MTC and the replisome. Proceedings of the National Academy of Sciences of the United States of America, 114 (40), 10630-10635.

Single-molecule visualization of Saccharomyces cerevisiae leading-strand synthesis reveals dynamic interaction between MTC and the replisome

Abstract

The replisome, the multiprotein system responsible for genome duplication, is a highly dynamic complex displaying a large number of different enzyme activities. Recently, the *Saccharomyces cerevisiae* minimal replication reaction has been successfully reconstituted in vitro. This provided an opportunity to uncover the enzymatic activities of many of the components in a eukaryotic system. Their dynamic behavior and interactions in the context of the replisome, however, remain unclear. We use a tethered-bead assay to provide real-time visualization of leading-strand synthesis by the *S. cerevisiae* replisome at the single-molecule level. The minimal reconstituted leading-strand replisome requires 24 proteins, forming the CMG helicase, the Pol e DNA polymerase, the RFC clamp loader, the PCNA sliding clamp, and the RPA single-stranded DNA binding protein. We observe rates and product lengths similar to those obtained from ensemble biochemical experiments. At the single-molecule level, we probe the behavior of two components of the replication progression complex and characterize their interaction with active leading-strand replisomes. The Minichromosome maintenance protein 10 (Mcm10), an important player in CMG activation, increases the number of productive replication events in our assay. Furthermore, we show that the fork protection complex Mrc1-Tof1-Csm3 (MTC) enhances the rate of the leading-strand replisome threefold. The introduction of periods of fast replication by MTC leads to an average rate enhancement of a factor of 2, similar to observations in cellular studies. We observe that the MTC complex acts in a dynamic fashion with the moving replisome, leading to alternating phases of slow and fast replication.

Disciplines

Medicine and Health Sciences

Publication Details

Lewis, J. S., Spenkelink, L. M., Schauer, G. D., Hill, F. R., Georgescu, R. E., O'Donnell, M. E. & van Oijen, A. M. (2017). Single-molecule visualization of Saccharomyces cerevisiae leading-strand synthesis reveals dynamic interaction between MTC and the replisome. Proceedings of the National Academy of Sciences of the United States of America, 114 (40), 10630-10635.

Authors

Jacob S. Lewis, Lisanne Spenkelink, Grant D. Schauer, Flynn R. Hill, Roxanna E. Georgescu, Michael E. O'Donnell, and Antoine M. van Oijen

Title Page.

Classification: BIOLOGICAL SCIENCES: Biochemistry; Biophysics and Computational Biology; Cell Biology.

Title: Single-molecule visualization of *S. cerevisiae* leading-strand synthesis reveals dynamic interaction between MTC and the replisome.

Authors: Jacob S. Lewis[a,1], Lisanne M. Spenkelink[a,b,1], Grant D. Schauer[c], Flynn R. Hill[a], Roxanna E. Georgescu[c], Michael E. O'Donnell[c] and Antoine M. van Oijen[a]

[1]These authors contributed equally

Author Affiliation: [a] Centre for Medical & Molecular Bioscience, University of Wollongong, and Illawarra Health & Medical Research Institute, Wollongong, NSW 2522, Australia. [b] Zernike Institute for Advanced Materials, University of Groningen, 9747 AG Groningen, the Netherlands. [c]Howard Hughes Medical Institute and Rockefeller University, New York, NY 10065.

Corresponding Authors:
Antoine M. van Oijen
University of Wollongong
Wollongong, NSW 2522, Australia
+61 2 4221 4780
vanoijen@uow.edu.au

Michael E. O'Donnell
Rockefeller University
New York, NY 10065
212-327-7255
Michael.O'Donnell@rockefeller.edu

Keywords: DNA replication, single-molecule biophysics, replisome, CMG, Mrc1, Claspin, Tof1.

Abstract. The replisome, the multi-protein system responsible for genome duplication, is a highly dynamic complex displaying a large number of different enzyme activities. Recently, the *Saccharomyces cerevisiae* minimal replication reaction has been successfully reconstituted in vitro and provides an opportunity to uncover the enzymatic activities of many of the components in a eukaryotic system. Their dynamic behavior and interactions in the context of the replisome, however, remain unclear. We use a tethered-bead assay to provide real-time visualization of leading-strand synthesis by the *S. cerevisiae* replisome at the single-molecule level. The minimal reconstituted leading-strand replisome requires 24 proteins, forming the CMG helicase, the Pol ε DNA polymerase, the RFC clamp loader, the PCNA sliding clamp and the RPA single-stranded DNA binding protein. We observe rates and product lengths similar to those obtained from ensemble biochemical experiments. At the single-molecule level, we probe the behavior of two components of the replication progression complex and characterize their interaction with active leading-strand replisomes. The Minichromosome maintenance protein 10 (Mcm10), an important player in CMG activation, increases the number of productive replication events in our assay. Furthermore, we show that the fork protection complex Mrc1–Tof1–Csm3 (MTC) enhances the rate of the leading-strand replisome 3-fold. The introduction of periods of fast replication by MTC leads to an average rate enhancement of a factor of 2, similar to observations in cellular studies. We observe that the MTC complex acts in a dynamic fashion with the moving replisome, leading to alternating phases of slow and fast replication.

Significance Statement. Replication of genomic DNA is essential to all cells. The replisome, the multi-protein machine that performs DNA replication, contains many moving parts, the actions of which are poorly understood. Unraveling the dynamic behavior of these proteins requires novel application of single-molecule imaging techniques, to eliminate averaging inherent in ensemble methods and to directly observe short-lived events. Here, we present the first single-molecule observations of an active *S. cerevisiae* replisome using purified proteins. We find that a checkpoint complex (Mrc1–Tof1–Csm3), known to bind and to speed up the replisome, interacts only transiently with the replisome. This work represents a major step towards establishing the tools needed to understand the detailed kinetics of proteins within the complex eukaryotic replisome.

\body

The replisome is the molecular machine that coordinates the enzymatic activities required for genome duplication. It contains proteins responsible for DNA unwinding, depositing primers, synthesizing DNA, and coordinating DNA production on both strands. The replisome in eukaryotes is a sophisticated and highly regulated machine; its assembly is performed by origin-initiation proteins and kinases that restrict chromosome duplication to a single round to ensure proper ploidy across multiple chromosomes. Replisome operations must be finely tuned to adjust to changing cellular conditions and to interface with numerous repair pathways. While the minimal operating machinery to advance a replication fork has been established in vitro (1, 2), the reactions were unable to achieve rates measured in vivo. This deficiency is not surprising considering the several additional proteins that move with replisomes in vivo (3, 4). The evolution of checkpoints has provided eukaryotic cells with surveillance mechanisms that orchestrate the recruitment of many other proteins to replication forks that modulate replisome activity. Using simplified in vitro assays, study of these additional proteins has resulted in the reconstitution of efficient leading- and lagging-strand DNA replication on naked and chromatinized templates in vitro (1, 3-7).

Once CMG helicase and the Pol ε leading-strand DNA polymerase (together called CMGE) are assembled at the replication fork, additional proteins are conscripted to the complex to form the RPC. These proteins include Ctf4, Csm3, FACT, Mrc1, Pol α, Tof1, and Top1 (8). It

has been shown that Mrc1, a yeast homolog of Claspin and an S-phase specific mediator protein of the DNA damage response, is recruited to the fork (8, 9) and increases the rate of replication in vivo about 2-fold (10-12). In vitro studies confirm that Mrc1 increases the speed of replication forks to rates similar to those measured in vivo (5). inclusion of Csm3/Tolf1 stimulated the functional association of Mrc1 with the replisome. Mrc1 binds both the N- and C-terminal halves of Pol2, the polymerase/exonuclease of Pol ε (13). Given that we have only begun to determine the exact roles of the individual proteins at the fork, understanding basic mechanisms during DNA replication that coordinate enzymatic activity has thus far been very challenging. To date, all in vitro methods used to study *S. cerevisiae* DNA replisome activity have relied on traditional biochemical techniques (1-5, 7). Such experiments have provided the molecular mechanisms that target the replicative polymerases to their respective strands during bulk DNA synthesis (1-3, 14). However, these ensemble methods only report averages of total DNA synthesis. The dynamic behaviors that actually govern transitions through multiple conformational states, driven by a hierarchy of strong and weak interactions, are inaccessible using traditional biochemical assays. This knowledge is essential to understand these processes in biophysical detail. Single-molecule based approaches of DNA replication allow real-time observation of individual replisomes, revealing rare intermediates and often surprising dynamics during replication that cannot be otherwise detected (15-17).

Here, we use single-molecule tethered-bead assays to study the kinetics of the leading strand replisome of a eukaryote, which has homologous replication machinery to that used in human. The minimal replisome system is reconstituted from the helicase complex Cdc45, MCM2–7, GINS (CMG), the leading-strand DNA Pol ε, the clamp loader Replication Factor C (RFC), the sliding clamp Proliferating Cell Nuclear Antigen (PCNA) and single-stranded DNA (ssDNA) binding protein (SSB). In the current report we observe synthesis of the leading strand in real time at rates consistent with cellular observations. In the presence of Minichromosome maintenance protein 10 (Mcm10), we observe a 3-fold increase in the number of productive replication events and an increase in the basal rate of the minimal replisome, supporting the role of Mcm10 in fork rate and stability after origin firing (6). Mrc1 forms a complex with Tof1 and Csm3, referred to as the MTC fork protection complex. The MTC complex is generally thought to function when the replication fork is challenged with DNA damage or at replication fork barriers (8, 9, 18). In the presence of MTC we observe significantly increased rates of replication, consistent with values previously published (5), and observations that MTC regulates fork speed in the cell (13). Unexpectedly, the MTC complex causes multiple changes in rate over time during a single leading-strand replication reaction observed at the single-molecule level. In sum, the observations documented herein show a highly dynamic interaction between MTC and the leading-strand replisome.

Results.

Single-molecule visualization of leading-strand synthesis. We use a single-molecule tethered-bead flow-stretching assay (19, 20) to directly visualize the replication kinetics of individual *S. cerevisiae* leading-strand replisomes. A linear and double-stranded DNA substrate (Fig. S1) containing a replication fork is attached to a microbead on one end and the surface of a microscope cover slip on the other (Fig. 1 *C*). We apply a laminar flow to exert a controllable drag force on the beads, and thus stretch out the DNA molecules. We use ultra-wide-field, low-magnification microscopy to image thousands of beads and relate bead movement to changes in DNA length (17) (Fig. 1 *A* and *B*). At drag forces lower than 6 pN, ssDNA is approximately six times shorter than double-stranded DNA (dsDNA) (19, 21). Movement of the bead against the direction of flow, therefore, reports on the conversion from dsDNA to ssDNA. With leading-strand synthesis effectively converting parental DNA into ssDNA on the lagging strand, we can now monitor leading-strand synthesis by a gradual

shortening of individual DNA molecules. Topoisomerase is not required because the DNA is free to rotate at both ends, thus preventing accumulation of supercoils. Automated fitting of the bead images and tracking of the bead positions as a function of time provides a read out for these interconversions with high precision (~50 nm, corresponding to ~200 bp; (17)). Simultaneously tracking thousands of beads enables high data throughput and the characterizations of sub populations within individual experiments. We can characterize properties of individual replisomes such as rate (and changes therein) and the product length (the total number of nucleotides synthesized per replisome during the experiment).

To recapitulate previous in vitro (2) results at the single-molecule level, we visualized leading-strand DNA synthesis using the single-molecule tethered-bead flow-stretching assay (Fig. 1 *D*). The biotinylated fork is tethered to the streptavidin coated surface of the flow cell and the digoxigenin couples to a 2.8-μm, anti-digoxigenin coated bead ((Materials and Methods)). The leading-strand arm of the fork contains a 3' ssDNA tail that is exposed to the solution to facilitate loading of CMG helicase

Measuring the length difference between ssDNA and dsDNA provides a ratio between the number of processed nucleotides by the DNA polymerase and the amount of observed shortening. Due to the presence of ssDNA binding protein the measured contour length of ssDNA will be higher than that for naked ssDNA. To correct for this difference, we measured the change in ssDNA length upon RPA binding and the ratio was derived between the lengths of dsDNA and RPA-coated ssDNA (Fig. S2). This value was 106 ± 10 %, making RPA-coated ssDNA almost the same length as dsDNA. RPA is therefore incompatible with the visualization of changes in DNA length during leading-strand synthesis. Consequently, we used *E. coli* SSB in all replication assays, as ssDNA coated with SSB has a contour length that is 24 ± 2 % that of dsDNA, corresponding to an experimental conversion factor of 5596 ± 73 nt/μm (Fig. S2). *E. coli* SSB and *S. cerevisiae* RPA give indistinguishable results in the leading-strand synthesis reaction (Fig. S3).

Single-molecule replication rates of Pol ε-dependent leading-strand synthesis. The experimental strategy for establishing the leading-strand replisome is outlined in Fig. 1 *D*. First, CMG is loaded onto the fork under a flow of buffer. Subsequently, leading-strand synthesis is initiated by introducing a flow of buffer containing CMG, Pol ε, PCNA, RFC, PCNA, Mg^{2+}, all four dNTPs and ATP (See Materials and Methods for precise details). Fig. 2 *A* shows length changes of two individual DNA molecules as a function of time. A gradual shortening of the DNA is clearly visible, indicating sustained conversion of dsDNA into ssDNA. To detect rate changes and to identify different operational modes of the leading-strand replisome, we used an unbiased, multiline-fitting algorithm based on change-point theory (17, 22) (Fig. 2 *A*, black lines). The rates obtained from this algorithm are weighted by the DNA segment length, reflecting the number of nucleotides that were synthesised at this rate. This places more significance to the longer rate segments, as they have a higher signal-to-noise ratio compared to shorter ones. The rate was determined by fitting the rate histogram with a Gaussian function, resulting in a rate of 5.4 ± 0.7 nt/s (mean ± s.e.m) (Fig. 2 *B*), consistent with earlier ensemble reactions using ^{32}P-dNTPs (2). The rate values in these single-molecule experiments are consistent with previously reported ensemble experiments (1, 2) and use of yeast extracts in single-molecule experiments (23). Instead of using processivity, a term that is ambiguous in definition when comparing experiments with very different protein and DNA concentrations, we leverage the precise nature of our single-molecule measurements to define the product length of individual DNA products. The overall product length for an experiment is determined by measuring the total amount of dsDNA converted into ssDNA for every trajectory and fitting their distribution with a single-exponential decay (assuming a single rate-limiting step determining the end of an event). The product length of Pol ε-dependent leading-strand synthesis was measured to be 0.9 ± 0.2 kilonucleotides (knt) in the 20-minute observation time (Fig. S4 *A*). These rate values for

a minimal leading-strand replisome are consistent with previously reported ensemble experiments (1, 2). In the absence of the four dNTPs no replication events were observed, demonstrating that the observed bead movements are enzyme dependent. We note that previous ensemble assays of recombinant CMG show that CMG binds DNA for up to one hour, and that these longer time windows enable CMGE–PCNA to eventually complete synthesis of a 3-kb template (1-3). In our current setup, however, the typical observation time is 20 minutes, and we cannot directly observe when enzyme binding and/or unbinding occurs. The processivity/stability of these components on DNA and proficiency to exchange with components from solution will be the subject of a future study.

To exclude the possibility of Pol ε-independent unwinding of dsDNA by CMG, we performed the experiment in the absence of Pol ε. As expected, we do not see any replication events (Fig. 2 *A*). We also performed the experiment lacking CMG, but detect no replication events, consistent with inability of Pol ε to strand-displace. Combining these results, we conclude that the effective shortening of the DNA substrate arises from CMG–Pol ε dependent leading-strand synthesis. This observation provides us with the ability to monitor leading-strand replication of *S. cerevisiae* in real time at the single-molecule level. Additionally, it affords us the opportunity to characterize interactions between proteins within the leading-strand replisome, one replisome at a time.

Mcm10 increases the number of productive replication events. Mcm10 has been identified as an important player in CMG activation (24, 25) and maintenance of the replication fork (26). Studies using reconstituted purified proteins have demonstrated that Mcm10 is not absolutely required for leading/lagging strand fork function in vitro (1). To understand the effect of Mcm10 during leading-strand replication at the single-molecule level, we added equimolar amounts of CMG and Mcm10 during initial CMG loading and in the subsequent replication reaction. The addition of Mcm10 did not result in any Pol ε-independent unwinding of dsDNA by CMG. However, addition of Mcm10 to the leading-strand replication reaction resulted in an average of 1.3-fold increase in rate (11.0 ± 0.6 nt/s, Fig. 3 *B*), consistent with previous ensemble observations (6). Interestingly, we did notice a significant ~3-fold increase in the number of trajectories that show replication events (Fig. *2 C*). The efficiency is defined as a percentage of the number of correctly tethered beads that show replication. The average number of correctly tethered beads is 981 ± 147 (N = 5 experiments). This increase in efficiency suggests that Mcm10 facilitates the assembly of an active leading-strand complex, or enhances its stability as observed earlier (6). Consequently, all further single-molecule experiments included Mcm10.

Addition of MTC increases replication rates of Pol ε-dependent leading-strand synthesis. Previous studies demonstrated that MTC is required for maximal fork speed in vivo (10, 12, 13), and in vitro (5). The in vitro ensemble experiments, however, did not inform on the lifetime of MTC binding to a leading-strand replisome or on its effect on the instantaneous replication rates. The Mrc1, Tof1 and Csm3 proteins are present in the RPC in a substoichiometric fashion, suggesting they are not present in every replisome or only transiently associated (8). To provide access to this important kinetic information, we repeated the tethered-bead assay in the presence of 30 nM MTC (Fig. 3 *A*). We observe a 2-fold increase in average replication rate (19.7 ± 1.2 nt/s) in the presence of MTC consistent with in vivo observations of fork speed in the presence and absence of Mrc1 (Fig. 3 *B*), and an increase in product length (compare Fig. S4 *B* with Fig. S4 *C*). The overall 1.8-fold rate increase is consistent with several in vivo studies of Mrc1 deficient cells (10-12). Previous work reported that Mrc1 is responsible for the increased fork speed, even though the interaction of MTC with the replisome is largely mediated by Tof1, and that Mrc1 function is largely aided by the presence of Tof1 (5, 8, 12, 13, 18). Consistent with this observation, the increase in leading-strand fork speed we observe requires MTC and is not observed using

only the (Tof1–Csm3) TC complex. Leading-strand replication performed in the presence of the TC complex, resulted in the loss of the higher rates and loss of the increase in product length compared to the MTC complex that includes Mrc1 (Fig. 3 *B,* and*E*, and Fig. S4 *D*).

MTC induces multiple rate changes within a single leading-strand replication complex. The single-molecule rate distribution for MTC-mediated leading-strand synthesis shows a bimodal rate distribution, comprised of a slow population with a rate of 7.4 ± 0.2 nt/s (mean ± s.e.m) and a fast population with a rate of 21.1 ± 0.7 nt/s. While these observations appear to suggest an unsaturated reaction, we have titrated MTC into bulk assays from 0–120 nM MTC and observe saturation at 15 nM, less than the 30 nM MTC used in the experiments of this report (Fig. S5). The appearance of these two populations highlights the importance of using single-molecule techniques, as this bimodal distribution would not be visible in traditional ensemble-averaging assays. This bimodal distribution can be explained by two possible mechanisms — one in which MTC speeds up a subset of replisomes, or one in which MTC interacts with all replisomes, but only transiently. If the first mechanism were true, a subset of trajectories would exhibit faster rates consistent with these replisomes associated with MTC, whereas the rest would exhibit the slow rate observed in the absence of MTC. If the second mechanism were true, we should see both slow and fast rates within a single trajectory, resulting in multiple rate changes per replisome. To distinguish between these two possibilities, we first quantified the number of rate changes for each replisome. Rate changes were defined by the change-point line-fitting analysis (Fig. S6). On average we observe 4.5 times more rate changes when MTC is present (Fig. 4 *A*). This high frequency of rate changes within individual reactions identifies that MTC interacts with all replisomes, but only transiently.

Furthermore we examined the distribution of rates associated with individual switches between rates. We did so by plotting the rate of a change-point segment within a single-molecule trace, versus the rate of the previous change-point segment in the same trajectory (Fig. 4 *B*). The points in this transition plot represent rate pairs from trajectories with multiple rate changes. While we do observe some rate changes in the absence of MTC (Fig. 4 *B* top), the points in the transition plot are clustered close to the diagonal. This clustering indicates that the rate changes are only minor, and are probably due to the small intrinsic rate variations of Pol ε–dependent synthesis. In contrast, when MTC is present the points in the transition plot lie much further away from the diagonal (Fig. 4 *B* bottom). This deviation from the diagonal shows that the change in the rate between two segments in a single trajectory is large. These large changes imply that the replisome can transition from fast, MTC-mediated rates to the slow rates, and vice versa. To quantify the average change in rate between transitions within a single trajectory, we calculated the average distance from the diagonal for all the points in the transition plot. In the presence of MTC the average rate change is ~2.5-fold higher with a rate change of 13.6 ± 1.1 nt/s (mean ± s.e.m) compared to 5.9 ± 0.6 nt/s in the absence of MTC. Moreover, the fact that the off-diagonal points are symmetrically distributed around the diagonal illustrates that it is just as likely for a slow rate segment to be followed by a fast rate segment, as it is for a fast rate segment to be followed by a slow one. This lack of bias reveals that MTC can bind and unbind from the replisome after replication has started. This observation further supports that MTC undergoes cycles of binding to the replisome from solution, and dissociation. We verified that placing the 3XFLAG tag on the C-terminus of Mrc1 and no tag on Csm3 within MTC instead of the N-terminal FLAG–Mrc1 (i.e. compared to use of a C-terminal FLAG tag on Mrc1 and a C-terminal calmodulin tag on Csm3 in (5, 7)) did not result in appreciable differences in the ability of MTC to induce multiple rate changes within single leading-strand replication complexes (Fig. S7).

MTC is transiently associated to the CMGE leading-strand replication fork complex. We reasoned that if MTC is indeed weakly bound to the replisome, we should be able to decrease the frequency of rate transitions by lowering the concentration of MTC. Replication reactions performed in the presence of either 10 nM or 3 nM MTC, showed a reduction in the number of fast rates as well as the frequency of transitions within a single trajectory (Fig. S8). To extend these observations, we performed leading-strand synthesis under conditions permitting preassembly of replisomes at the fork. If indeed MTC transiently associates with the replisome, we should not see the faster rates when we include MTC during the assembly phase, but omit it from the subsequent replication reaction, as it would dissociate by the time the replication reaction started. As predicted, the rate distribution did not show the fast population (Fig. 4 *C*). In contrast, when the CMGE complex is assembled on DNA and Pol ε is omitted from the subsequent replication reaction but MTC is present in the buffer flow, the faster population is evident (Fig. 4 *D*). This result indicates that Pol ε remains stably bound to the replisome, consistent with previous reports (3). Combining these results, we hypothesize that MTC has a weak affinity for the leading-strand replisome and interacts in a dynamic fashion to increase the rate of the replication fork.

Discussion.

We have used a DNA-stretching assay to visualize in vitro leading-strand synthesis by the *S. cerevisiae* replisome at the single-molecule level. Similar experiments have been reported for the T7 and *E. coli* replisomes (17, 20, 27, 28), but a detailed kinetic analysis of the eukaryotic replisome at the single-molecule level has been unavailable thus far. The leading-strand synthesis rates observed here are similar to those previously reported in ensemble biochemical reactions (1, 5) and within the range of replication fork movement observed inside the cell (12, 29, 30). This assay has allowed us to probe the effect of Mcm10 and MTC on leading-strand replisome activity, confirming reports that Mcm10 stimulates the minimal replisome in the absence of MTC (6), and that MTC stimulates the replisome rate by an average of 1.8-fold, as summarized in Fig. 5. The observations of Mrc1 dependent stimulation of fork rate are also consistent with cell biology studies of fork movement in Mrc1 cells (10-12). Interestingly, observation at the single-molecule level has revealed unexpected kinetic behaviors that would have been impossible to observe with conventional biochemical assays.

We observe that Mcm10 does not substantially increase the rate or product length of leading-strand synthesis, but does increase the number of productive replication events, consistent with a recent study indicating that Mcm10 stabilizes the CMG on DNA (6). This Mcm10 associated increase in efficiency could be relevant to the conclusions that Mcm10 functions as an activator of the CMG complex throughout DNA replication (6, 31), assisting stabilization of CMG or helping it overcome possible obstacles. Mcm10 is also known to activate Mcm2–7 during replication initiation (24, 32, 33). It is conceivable that Mcm10 helps activate Mcm2–7 in our in vitro leading-strand system through a similar mechanism. It also remains possible that Mcm10 stabilizes Pol ε or otherwise enhances its synthesis activity.

The current study demonstrates that the MTC complex increases the rate of leading-strand synthesis in an unexpected fashion (summarized in Fig. 5 *C*). The MTC complex appears to act in a highly dynamic fashion, only transiently active at the replisome. This observation is consistent with the substoichiometric presence of these subunits in the RPC complex (34). We observe processive leading-strand reactions at the single-molecule level with short-lived phases of higher rates that we interpret as corresponding to MTC binding to the replisome. Interestingly, the instantaneous rate during these phases increases by 3-fold, but average out to an approximately 2-fold average rate increase because they do not persist throughout the entire trajectory of an individual replisome. Further, the 2-fold average rate increase is consistent with observations of Mrc1 in the cellular context (10-12). The fluctuating rates per single-molecule trajectory suggest that MTC is distributive, and does not bind to the

replisome in a stable manner. Distributive behavior of critical replisome components has precedent in bacterial DnaG primase (35). When we compare the rates of successive segments within one trajectory we see that fast MTC-mediated rates can be followed by slow rates and vice versa. Furthermore, the amplitude of these rate changes is on average ~2.5 fold higher than the rate changes without MTC. This observation demonstrates that MTC or one of its components (e.g. Mrc1) associates with and dissociates from the replisome multiple times during leading-strand synthesis. The fact that we do not observe any fast rates when MTC is omitted during the replication phase, but present during the CMG loading phase of a preassembly experiment, further supports the conclusion that transient interactions exist between MTC and the replisome. These data contrast with previous models that suggest that Mrc1 stably binds to both CMG and Pol ε (8), though we note that cross-linking in ChIP assays prevents dynamics, and pull downs are not quantitative. It was proposed that this pair of interactions could be responsible for the faster rates, by tethering Pol ε to CMG (13, 36). The higher kinetic resolution of our experiments reveals the dynamic interaction of MTC with the replisome, with the population-averaged observables consistent with earlier biochemical assays. From the current study, however, we cannot conclude whether MTC acts to stimulate the DNA polymerase or the rate of unwinding, or both.

It is important to note that the exact phosphorylation state of the proteins is expected to play a role in MTC–replisome interactions (37). In addition, the current study focuses on the enzymes of leading-strand synthesis while additional proteins could play a role in MTC behavior. Replication proteins in *S. cerevisiae* undergo many post-translational modifications before and during replication (38, 39). For example, Dbf4-dependent kinase (DDK) and (cyclin-dependent kinase) CDK are known to control replication initiation by phosphorylation of many proteins involved in forming the origin recognition complex (39, 40). Additionally, phosphorylation of replisome components plays an important role in programmed fork arrest through phosphorylation of Mcm2–7, which promotes recruitment of Tof1–Csm3 by the replisome (37). *S. cerevisiae* recombinant expressed CMG and Tof1–Csm3 are phosphoproteins that facilitate their interaction (37). Interestingly, upon co-expression of CMG the vast majority of expressed proteins are free Mcm2–7, Cdc45 and GINS that do not simply self-assemble into a CMG complex (40). Thus, it is possible that the small amount of recombinant CMG recovered from expression cells is in fact assembled at origins (2). We note that Mrc1 has previously been shown to be the only component of MTC that enhances replisome rate (5) and since our observations rely on the conversion of dsDNA to ssDNA, it is possible that the dynamic interactions reported herein are of Mrc1 instead of the entire MTC complex.

It is tempting to speculate a possible biological reason for a dynamic interaction of Mrc1/MTC with the replisome. We presume that the different replication rates that correspond to the association state of Mrc1/MTC reflect different conformations of the replisome. Different replisome conformations may in turn facilitate active site configurations (i.e. enzymatic velocities), additional protein interactions or exchange with other partners, in a differential manner. An interesting aspect of MTC activity is its phosphorylation state. For example, it is well known that Mrc1 mediates the DNA-damage response through phosphorylation of Mrc1 by the Mec1/Rad53 kinases (41). The advantage of a dynamic interaction of Mrc1/MTC with CMG could provide an interesting type of regulation. The dynamic interaction between MTC and the replisome documented herein could ensure a complete sampling of the phosphorylation state of MTC by all replisomes, as opposed to only a subset of replisomes carrying a fully phosphorylated MTC complex. A dynamic mechanism of MTC–replisome interaction would allow the MTC to act as a potentiometer for damage. The ratio of modified and unmodified MTC (i.e. in response to DNA damage) would be “sensed” by all replisomes equally, instead of a stark division in the case of a stable interaction of MTC with CMG, which would result in different fork speeds within the same cell. Hence, a dynamic interaction would provide a gradual titration of phosphorylated MTC, equally sampled by all replisomes, and consequently provide a more uniform fork speed.

Despite these studies revealing the dynamic nature of MTC within a replisome, future studies are required to understand how replication proteins interact in vitro and in living cells.

Materials and Methods.

Protein expression and purification. CMG, Pol ε, RFC, PCNA, RPA and SSB were purified as described (2). Purification of Mcm10 and MTC are in Supporting Information.

Linear fork DNA substrates.

DNA replication templates used in ensemble leading-strand experiments were prepared as described (2, 14). The replication substrate used for surface tethering and bead attachment in single-molecule experiments was constructed using a 19,979 bp PCR λ-phage product and the HPLC purified oligonucleotides listed in Table S1 (Integrated DNA Technologies). See Supporting Information for full details.

Single-molecule tethered bead assay. Flow cells were prepared as described (17, 42). First, CMG was loaded at the fork using 30 nM CMG, 30 nM Mcm10, and MTC (where indicated) in replication buffer (25 mM Tris-HCl pH 7.6, 10 mM Mg acetate, 50 mM K glutamate, 40 μg/ml BSA 0.1 mM EDTA, 5 mM DTT and 0.0025% (v/v) Tween-20) at 15 μL/min for 10 min. Reactions were initiated by introducing 30 nM CMG, 30 nM Mcm10, 40 nM Pol ε , 20 nM PCNA, 6 nM RFC, 250 nM *E. coli* SSB and MTC (where indicated) in replication buffer supplemented with 5 mM ATP and 60 μM dCTP, dGTP, dATP, and dTTP. See Supporting Information for full details.

Ensemble leading-strand replication assays. Replication reactions (25 μL) contained 25mM Tris-acetate pH 7.5, 5% (v/v) glycerol, 40 μg/ml BSA, 3 mM DTT 2mM tris(2-carboxyethyl)phosphine, 10 mM Mg acetate, 50 mM K glutamate, 0.1 mM EDTA, 5 mM ATP, and 120 μM of each dNTP unless otherwise noted. See Supporting Information for full details.

Code availability. Source code for most analysis tools is available at GitHub under Single-Molecule Biophysics beadpy, or upon request.

Acknowledgments.

We are grateful to Olga Yurieva and Dan Zhang for MTC, Pol ε, CMG, Mcm10, and to Karl Duderstadt for single-molecule analysis software. Research was supported by the Australian Research Council: DP150100956 and Australian Laureate Fellowship to A.M.v.O. (FL140100027), Fundamenteel onderzoek der materie (FOM) for L.M.S (12CMCE03), and NIH GM-115809 and HHMI for G.S. and M.E.O.

Author contributions.

J.S.L, L.M.S, G.D.S., R.E.G., M.E.O. and A.M.v.O designed research; J.S.L and L.M.S. performed single-molecule experiments. G.D.S. performed ensemble experiments; J.S.L, L.M.S, G.D.S analyzed data; F.R.H wrote the beadpy Python software, G.D.S. and R.E.G provided reagents; J.S.L, L.M.S, G.D.S., M.E.O. and A.M.v.O wrote the manuscript.

References.

1. Georgescu RE, et al. (2015) Reconstitution of a eukaryotic replisome reveals suppression mechanisms that define leading/lagging strand operation. *eLife* 4:e04988.

2. Georgescu RE, et al. (2014) Mechanism of asymmetric polymerase assembly at the

eukaryotic replication fork. *Nat Struct Mol Biol* 21(8):664–670.

3. Langston LD, et al. (2014) CMG helicase and DNA polymerase ε form a functional 15-subunit holoenzyme for eukaryotic leading-strand DNA replication. *Proc Natl Acad Sci U S A* 111(43):15390–15395.

4. Devbhandari S, Jiang J, Kumar C, Whitehouse I, Remus D (2017) Chromatin Constrains the Initiation and Elongation of DNA Replication. *Mol Cell* 65(1):131–141.

5. Yeeles JTP, Janska A, Early A, Diffley JFX (2017) How the eukaryotic replisome achieves rapid and efficient DNA replication. *Mol Cell* 65(1):105–116.

6. Lõoke M, Maloney MF, Bell SP (2017) Mcm10 regulates DNA replication elongation by stimulating the CMG replicative helicase. *Genes Dev* 31(3):291–305.

7. Kurat CF, Yeeles JTP, Patel H, Early A, Diffley JFX (2017) Chromatin controls DNA replication origin selection, lagging-strand synthesis, and replication fork rates. *Mol Cell* 65(1):117–130.

8. Katou Y, et al. (2003) S-phase checkpoint proteins Tof1 and Mrc1 form a stable replication-pausing complex. *Nature* 424(6952):1078–1083.

9. Alcasabas AA, et al. (2001) Mrc1 transduces signals of DNA replication stress to activate Rad53. *Nat Cell Biol* 3(11):958–965.

10. Tourriere H, Versini G, Cordon-Preciado V, Alabert C, Pasero P (2005) Mrc1 and Tof1 promote replication fork progression and recovery independently of Rad53. *Mol Cell* 19(5):699–706.

11. Szyjka SJ, Viggiani CJ, Aparicio OM (2005) Mrc1 is required for normal progression of replication forks throughout chromatin in S. cerevisiae. *Mol Cell* 19(5):691–697.

12. Hodgson B, Calzada A, Labib K (2007) Mrc1 and Tof1 regulate DNA replication forks in different ways during normal S phase. *Mol Biol Cell* 18(10):3894–3902.

13. Lou H, et al. (2008) Mrc1 and DNA polymerase ε function together in linking DNA replication and the S phase checkpoint. *Mol Cell* 32(1):106–117.

14. Schauer GD, O'Donnell ME (2017) Quality control mechanisms exclude incorrect polymerases from the eukaryotic replication fork. *Proc Natl Acad Sci U S A* 114(4):675–680.

15. Lewis JS, et al. (2017) Single-molecule visualization of fast polymerase turnover in the bacterial replisome. *eLife* 6:e23932.

16. Geertsema HJ, van Oijen AM (2013) A single-molecule view of DNA replication: the dynamic nature of multi-protein complexes revealed. *Curr Opin Struct Biol* 23(5):788–793.

17. Duderstadt KE, et al. (2016) Simultaneous real-time imaging of leading and lagging strand synthesis reveals the coordination dynamics of single replisomes. *Mol Cell* 64(6):1035–1047.

18. Bando M, et al. (2009) Csm3, Tof1, and Mrc1 form a heterotrimeric mediator complex that associates with DNA replication forks. *J Biol Chem* 284(49):34355–34365.

19. van Oijen AM, et al. (2003) Single-molecule kinetics of λ exonuclease reveal base dependence and dynamic disorder. *Science* 301(5637):1235–1238.

20. Lee J-B, et al. (2006) DNA primase acts as a molecular brake in DNA replication. *Nature* 439(7076):621–624.

21. Bustamante C, Marko JF, Siggia ED, Smith S (1994) Entropic elasticity of lambda-phage DNA. *Science* 265(5178):1599–1600.

22. Watkins LP, Yang H (2005) Detection of intensity change points in time-resolved single-molecule measurements. *J Phys Chem B* 109(1):617–628.

23. Duzdevich D, et al. (2015) The dynamics of eukaryotic replication initiation: origin specificity, licensing, and firing at the single-molecule level. *Mol Cell* 58(3):483–494.

24. Perez-Arnaiz P, Bruck I, Kaplan DL (2016) Mcm10 coordinates the timely assembly and activation of the replication fork helicase. *Nucleic Acids Res* 44(1):315–329.

25. van Deursen F, Sengupta S, De Piccoli G, Sanchez-Diaz A, Labib K (2012) Mcm10 associates with the loaded DNA helicase at replication origins and defines a novel step in its activation. *EMBO J* 31(9):2195–2206.

26. Bielinsky A-K (2016) Mcm10: The glue at replication forks. *Cell Cycle* 15(22):3024–3025.

27. Tanner NA, et al. (2008) Single-molecule studies of fork dynamics in *Escherichia coli* DNA replication. *Nat Struct Mol Biol* 15(2):170–176.

28. Hamdan SM, et al. (2007) Dynamic DNA helicase-DNA polymerase interactions assure processive replication fork movement. *Mol Cell* 27(4):539–549.

29. Sekedat MD, et al. (2010) GINS motion reveals replication fork progression is remarkably uniform throughout the yeast genome. *Mol Syst Biol* 6:353.

30. Conti C, et al. (2007) Replication fork velocities at adjacent replication origins are coordinately modified during DNA replication in human cells. *Mol Biol Cell* 18(8):3059–3067.

31. Chadha GS, Gambus A, Gillespie PJ, Blow JJ (2016) Xenopus Mcm10 is a CDK-substrate required for replication fork stability. *Cell Cycle* 15(16):2183–2195.

32. Quan Y, et al. (2015) Cell-Cycle-Regulated Interaction between Mcm10 and Double Hexameric Mcm2-7 Is Required for Helicase Splitting and Activation during S Phase. *Cell Rep* 13(11):2576–2586.

33. Baxley RM, Bielinsky A-K (2017) Mcm10: A dynamic scaffold at eukaryotic replication forks. *Genes (Basel)* 8(2). doi:10.3390/genes8020073.

34. Gambus A, et al. (2006) GINS maintains association of Cdc45 with MCM in replisome progression complexes at eukaryotic DNA replication forks. *Nat Cell Biol* 8(4):358–366.

35. Tougu K, Marians KJ (1996) The interaction between helicase and primase sets the replication fork clock. *J Biol Chem* 271(35):21398–21405.

36. Labib K (2008) Making connections at DNA replication forks: Mrc1 takes the lead. *Mol*

Cell 32(2):166–168.

37. Bastia D, et al. (2016) Phosphorylation of CMG helicase and Tof1 is required for programmed fork arrest. *Proc Natl Acad Sci U S A* 113(26):E3639–48.

38. Siddiqui K, On KF, Diffley JFX (2013) Regulating DNA replication in eukarya. *Cold Spring Harb Perspect Biol* 5(9). doi:10.1101/cshperspect.a012930.

39. Bell SP, Labib K (2016) Chromosome duplication in *Saccharomyces cerevisiae*. *Genetics* 203(3):1027–1067.

40. Bruck I, Dhingra N, Kaplan DL (2017) A positive amplification mechanism involving a kinase and replication initiation factor helps assemble the replication fork helicase. *J Biol Chem* 292(8):3062–3073.

41. Zhou BB, Elledge SJ (2000) The DNA damage response: putting checkpoints in perspective. *Nature* 408(6811):433–439.

42. Geertsema HJ, Duderstadt KE, van Oijen AM (2015) Single-molecule observation of prokaryotic DNA replication. *Methods Mol Biol* 1300:219–238.

Figure Legends.

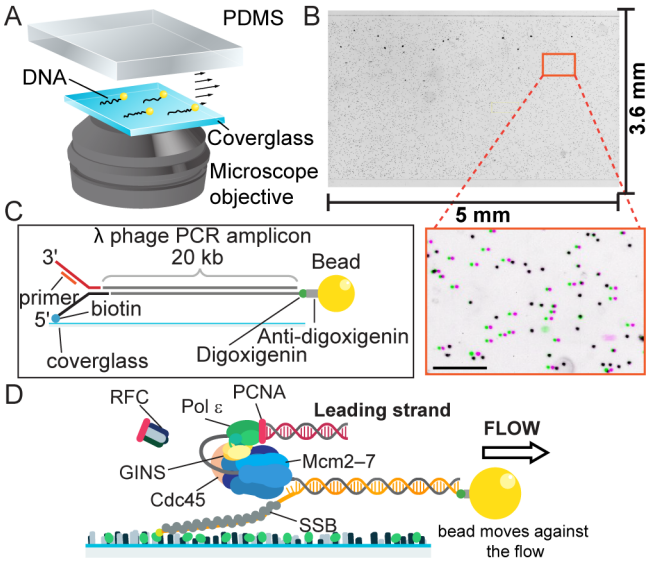

Fig. 1. Single-molecule tethered-bead DNA-stretching assay. (*A*) Experimental setup. DNA molecules are tethered in a microfluidic flow cell. Beads attached to DNA ends are imaged with wide-field optical microscopy. DNA molecules are stretched by applying a laminar flow of buffer. (*B*) A representative field of view showing 4,000 beads. (Inset) Image of beads attached to DNA flow-stretched in one direction (magenta) superimposed with an image of the same bead-attached DNA molecules stretched in the opposite direction (green) shows the presence of a large number of DNA-bead tethers. The beads that are improperly tethered are shown in black. The black scale bar is 150 μm. (*C*) DNA template. A replication fork was introduced at one end of a 20-kb linear substrate, with a bead attachment site at the other end. The fork is attached to the surface via a biotin on the 5′ tail. (*D*) Schematic of leading-strand replication by the minimal *S. cerevisiae* replisome. As dsDNA is converted into ssDNA, the DNA shortens and the bead moves against the direction of flow.

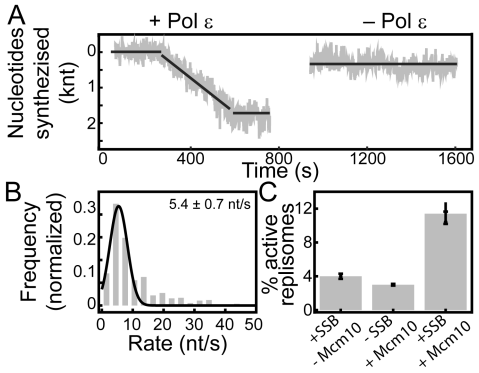

Fig. 2. Single-molecule visualization of leading-strand synthesis by *S. cerevisiae*. (*A*) Representative trajectories showing Pol ε-dependent leading-strand synthesis (left). When Pol ε is omitted no replication events are observed (right). The black lines represent the rate segments identified by the change-point algorithm. (*B*) Histogram of the instantaneous single-molecule rates. The black line represents a Gaussian fit with a rate of 5.4 ± 0.7 nt/s (mean ± s.e.m.) (*N* = 161 trajectories). (*C*) Efficiencies of leading-strand synthesis, defined as the number of beads that show replication events over the total number of correctly tethered beads. The efficiency is ~3-fold higher (11.4 ± 0.2 %, *N* = 3 experiments) in the presence of SSB and Mcm10,compared to experiments without Mcm10 (4.0 ± 0.3 %, *N* = 4

experiments) or without SSB (3.0 ± 0.1 %, *N* = 2 experiments). The errors represent the experimental error.

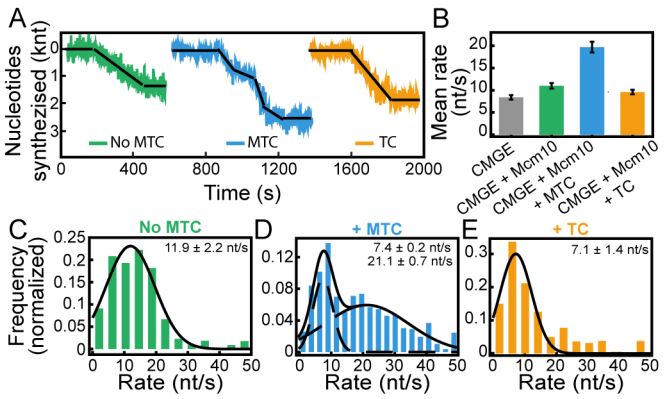

Fig. 3. Effect of MTC on replication kinetics. (*A*) Representative trajectories showing Pol ε-dependent leading-strand synthesis without MTC (left - green), with MTC (middle - blue), and with TC (right - orange). The black lines represent rate segments identified by the change-point algorithm. (*B*) Average single-molecule rates (mean ± s.e.m.), of all segments determined by the change-point algorithm, using CMGE (8.4 ± 0.5 nt/s), CMGE + Mcm10 (11.0 ± 0.6 nt/s), CMGE + Mcm10 + MTC (19.7 ± 1.2 nt/s) and CMGE + Mcm10 + TC (9.6 ± 0.5 nt/s). (*C*) Histogram of the instantaneous single-molecule rates for CMGE + Mcm10. The black line represents a Gaussian fit with a mean rate of 11.9 ± 2.2 nt/s, similar to the rates obtained without Mcm10 (Fig. 2*B*) (*N* = 96 trajectories). (*D*) Histogram of the instantaneous single-molecule rates for CMGE + Mcm10 + MTC. The histogram shows a bimodal distribution and was fit with the sum of two Gaussian distributions (black line), resulting in rates of 7.4 ± 0.2 nt/s and 21.1 ± 0.7 nt/s (*N* = 225 trajectories). (*E*) Histogram of the instantaneous single-molecule rates for replication by CMGE + Mcm10 + TC (omitting Mrc1). The fast population associated with MTC activity is not present (*N* = 111 trajectories).

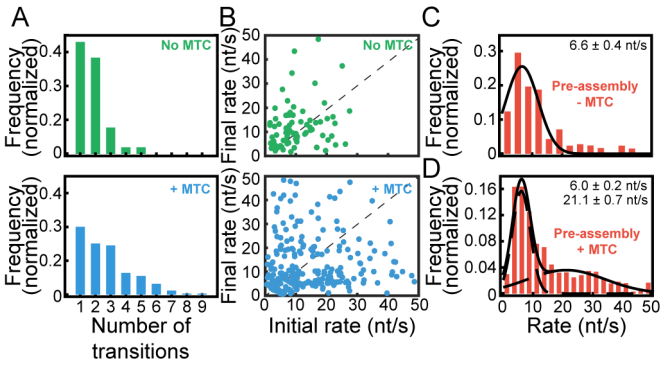

Fig. 4. MTC interaction with the replisome is transient. (*A*) The number of rate changes per trajectory without MTC (top) is 4.5 times lower than with MTC present (bottom). (*B*) Transition plots showing the rate of a segment as a function of the rate of the previous segment for trajectories with multiple segments, with (top) and without (bottom) MTC. The distance from the diagonal (dashed line) is ~2.5-fold higher with MTC (13.6 ± 1.1 nt/s, mean ± s.e.m) than without MTC (5.9 ± 0.6 nt/s, mean ± s.e.m.) (*C*) Histogram of the instantaneous single-molecule rates obtained with MTC was present during loading but omitted from the replication phase. The rate is 6.6 ± 0.4 nt/s, similar to the rates obtained in our continuous flow experiments without MTC. No MTC mediated fast rate population was observed (*N* = 101 trajectories). (*D*) Histogram of the instantaneous single-molecule rates obtained from an experiment where Pol ε was present during loading but omitted from the

replication phase. In contrast to the experiment in (*C*), the faster population is present. Fitting with the sum of two Gaussians gives rates of 6.0 ± 0.2 nt/s and 21.1 ± 0.7 nt/s (*N* = 196 trajectories).

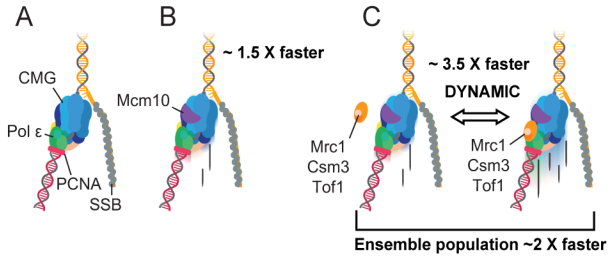

Fig. 5. Leading-strand synthesis by the *S. cerevisiae* replisome. (*A*) The minimal reconstituted leading-strand replisome supports leading-strand synthesis at a rate of 5.4 ± 0.7 nt/s. (*B*) Addition of Mcm10 increases the rate ~1.5 fold (11.9 ± 2.2 nt/s). (*C*) The MTC complex speeds up the leading-strand replisome by ~3.5 fold. Our single-molecule measurements demonstrate that MTC has a weak affinity for the replisome and only transiently interacts to speed up replication.

Supporting Information.

Purification of Mcm10 and MTC complex.

Mcm10: The gene encoding Mcm10 was amplified by PCR along with an N-terminal 10 histidine tag and a C-terminal 3X FLAG tag and cloned into pET-16b. *E.coli* cells (BL21-CodonPlus (DE3)-RIL) containing the dual tagged Mcm10 expression plasmid were grown to an OD_{600} of 0.6 (ampicillin and kanamycin resistant), induced with isopropyl β-D-1-thiogalactopyranoside (IPTG) for 18 h at 15°C, and collected and lysed using a pressure cell. Supernatant of lysed cells was applied to a 10 mL Chelating Sepharose Fast Flow (GE Healthcare) column charged with 50 mM nickel(II) sulfate and equilibrated with equilibration buffer (20 mM Tris-HCl pH 7.9, 5 mM imidazole, 500 mM sodium chloride, 0.01% (v/v) NP-40). After loading, the column was washed with equilibration buffer, then proteins were eluted in equilibration buffer containing 375 mM imidazole. Fractions were monitored by SDS-PAGE and peak fractions containing Mcm10 were applied to a 6 mL Anti-Flag M2 resin (Sigma) equilibrated in 20 mM Tris-HCl pH 7.5, 10% (v/v) glycerol, 500 mM sodium chloride, 1 mM dithiothreitol, 1 mM magnesium chloride, 0.01% (v/v) NP-40. After loading and subsequent washing with 50 mL equilibration buffer, the proteins were eluted using two 6 mL treatments of elution buffer containing 0.2 mg/mL 3X FLAG peptide (EZ Biolab) for 30 min. Fractions (100 µL) were collected and Mcm10 containing fractions were aliquoted, flash frozen in liquid N_2, and stored at –80°C (Figure S9).

Mrc1-Tof1-Csm3 complex: The genes encoding 3XFLAG-Mrc1 (^{Flag}Mrc1), Tof1 and 6xHis Csm3 (Csm3^{His}) were amplified from genomic DNA by PCR and inserted into yeast integration vectors similar as described for CMG in (1). Briefly, ^{Flag}Mrc1 was integrated at the *Ade2* locus, untagged Tof1 at the *His3* locus, and Csm1^{His} at the *Leu2* locus, each under control of the *Gal1/10* promoter. We also produced a yeast strain having a C-terminal Mrc1 3X FLAG tag and untagged Tof1, Csm3; the same procedure was used to purify both complexes (M_fTC; Figure S9). Cells were initially grown at 30°C in SC-glucose under selection and then they were divided into flasks containing YP-glycerol. Cell strains were grown at 30°C to OD_{600} of approximately 0.7, then induced by adding 20 g galactose/L for 6 h. After induction, cell pellets were collected by low speed centrifugation, resuspended in a minimal volume of 20 mM HEPES, pH 7.6, 1.2% (w/v) polyvinylpyrrolidone and flash frozen

by dripping into liquid N_2. Induced cells were lysed using a cryogenic grinding mill (SPEX), powder was thawed in the cold room and then resuspended in 250 mM potassium glutamate, 50 mM HEPES pH 7.5, 1 mM EDTA pH 8.0 plus protease inhibitors (P8215**,** Roche). Cell debris was removed by centrifugation at 4°C and the supernatant was mixed with 1.5 mL of anti-Flag M2 affinity resin (Sigma-Aldrich) for 1 h. The anti-FLAG resin was pelleted at 1000 × *g* and washed five times with 250 mM potassium glutamate, 50 mM HEPES pH 7.5, 1 mM EDTA pH 8.0 followed by centrifugation. Then the anti-Flag affinity resin was resuspended in 2 mL of buffer containing 250 mM potassium glutamate, 50 mM HEPES pH 7.5, 1 mM EDTA pH 8.0 containing 10% (v/v) glycerol. This protein solution was then loaded by gravity onto the same column and washed with buffer containing 250 mM potassium glutamate, 50 mM HEPES pH 7.5, 1 mM EDTA pH 8.0, 750 mM sodium chloride. The MTC complex was then eluted with the same buffer containing 0.2 mg/mL 3X FLAG peptide (EZ Biolab), but without sodium chloride. Eluted proteins were concentrated and further purified using a Superose 12 gel filtration column in 2X PBS containing 10% (v/v) glycerol. Fractions were analyzed by SDS-PAGE and MTC-containing fractions were flash frozen in liquid N_2 and stored at –80°C (Figure S9).

Single-molecule linear fork DNA substrates. The replication substrate used for surface tethering and bead attachment in single-molecule experiments was constructed using a 19,979 bp PCR λ-phage product and the HPLC purified oligonucleotides listed in Table S1 (Integrated DNA Technologies). Briefly, bacteriophage λ DNA (New England Biolabs) was used as a template for PCR. A *Nhe*I site and digoxigenin modification were incorporated using primers 20kbF and 20 kbR. Next, the PCR product was digested with *Nhe*I (New England Biolabs), and the enzyme was heat inactivated and concentrated by ethanol precipitation. To assemble the fork duplex, a 1:1 molar ratio of both complementary-fork arm and bio-fork arm oligonucleotides were annealed by heating to 94°C for 5 min in hybridisation buffer (10 mM HEPES pH 7.5, 5 mM magnesium acetate, 50 nM sodium chloride, 0.5 mM EDTA) in the presence of 1.5-fold molar excess of the C2 primer oligonucleotide. Next, a 1.1-fold molar excess of pre-formed fork duplex was ligated with the *Nhe*I-digested PCR fragment hybridisation buffer for 48 hours at 16 °C with 400 U of T4 DNA ligase (New England Biolabs). Linear fork substrates were diluted to 1.5 nM for subsequent use.

Single-molecule tethered bead assay. Flow cells were prepared as described previously (17, 42). All single-molecule tethered bead assays were performed at 30°C. Briefly, a PDMS lids was placed on top of a PEG-biotin-functionalized microscope slide (24 × 60 mm) to create a 3 mm wide and 100 µm high flow channel with Y junctions at both inlets and outlets. Polyethyleme tubes (PE-60: 0.76 mm inlet diameter and 1.22 mm outer diameter) were inserted to allow for a buffer flow. To help prevent non-specific interactions of proteins and DNA with the surface, the chamber was blocked with blocking buffer (20 mM Tris-HCl pH 7.5, 2 mM EDTA, 50 mM sodium chloride, 0.5 mg/ml BSA, and 0.0025% (v/v) Tween-20). The forked DNA substrates (20 pM) were flowed through the chamber for 12 min at 10 µL/min. After a brief wash with blocking buffer, tosylactivated paramagnetic beads (2.8 µm diameter, Life Technologies) functionalized with anti-digoxigenin (Roche) were introduced at 60 µL/min, until even surface coverage was achieved. Untethered beads were washed out of the chamber at 60 µL/min with ~600 µL of buffer. The leading-strand replication reaction was performed in stages. First, CMG was loaded at the fork by pre-loading 30 nM CMG, 30 nM Mcm10, and MTC (where indicated) in replication buffer (25 mM Tris-HCl pH 7.6, 10 mM magnesium acetate, 50 mM potassium glutamate, 40 µg/ml BSA 0.1 mM EDTA, 5 mM dithiothreitol and 0.0025% (v/v) Tween-20) at 15 µL/min for 10 min. Next, a magnet was introduced above the flow cell to limit surface interactions. Finally, replication reactions were initiated by introducing 30 nM CMG, 30 nM Mcm10, 40 nM Pol ε , 20 nM PCNA, 6 nM RFC,

250 nM *E. coli* SSB and MTC (where indicated) in replication buffer supplemented with 5 mM ATP and 60 μM dCTP, dGTP, dATP, and dTTP. The beads were illuminated with a fiber illuminator (Thorlabs) and movies were collected at 4 fps using a 29 megapixel CCD camera (Prosilica GX6600; Allied Vision Technologies; 5.5 μm pixel size) with StreamPix imaging software (NorPix) at 4 × magnification with a lens (TL12K-70-15; Lensation) mounted directly to the camera. Leading-strand replication was monitored over a period of 20 min by tracking the movement of the beads and converting changes in position to nucleotides using custom Python software programmed in house.

Bead selection and processing. Typical tethered bead experiments generated movies between 1000 and 10 000 beads per frame having file sizes of ~50 GB, making rapid and efficient data analysis challenging. Trajectories were selected using a highly-staged and automated set of processing steps. First, beads with high fitting error and those that could not be tracked were rejected. The remaining beads were further filtered to remove those that are immobile due to surface interactions, those that dissociated prior to enzymes reaching the flow cell, and those with any additional nearby beads influencing movement. Remaining beads were then analyzed for activity using kinetic change point analysis, and those with greater than 1000 nucleotides of total synthesis were kept. Remaining trajectories were corrected for instabilities in the flow by taking all the trajectories present from start to finish, centering these at zero, and then taking the median *x* and *y* positions at each time point. These are then boxcar smoothed to create a drift trajectory, which is subsequently subtracted from each trajectory. Next, these filtered trajectories were manually curated to remove those with bead movement greater than 0.3 μm in the transverse direction, those that do not have a clear start or end point, and those that start before enzymes have reached the flow cell. Regions of enzymatic activity were processed using kinetic change-point analysis using a global noise threshold (17, 22) and replication rates determined using the conversion factor derived in Fig. S2. Kinetic change-point segments containing less than 8 data points were also rejected.

Once all kinetic change points were determined, rate distributions were constructed using slopes from single change-point segments. Each rate was weighted by its segment length to attach more significance to the longer segments, as they have a higher signal-to-noise ratio compared to shorter ones. The Gaussian distributions were binned using the square-root rule to generate the final distributions seen in Figs. 2–4 and Fig. S7–8. Product-length histograms were generated using the total length of DNA synthesized in a single trajectory to produce the final distributions seen in Figs. 2–4 and Fig. S4, 7, 8. These distributions were fit with a single-exponential decay (assuming a single rate-limiting step determining the end of an event). All distributions were made and fitted using Matlab 2014b (Mathworks). The transition plots in Fig. 4 and Fig. S7–8 were generated by plotting the rate of a segment as a function of the rate of the previous segment, using only trajectories that have multiple rate segments.

Efficiency of leading-stand synthesis. The number of tethered beads was determined by counting the number of beads showing a proper flow reversal giving a length of 6.6 ± 0.1 μm (mean ± s.e.m). A typical experiment yielded 981 ± 147 correctly tethered beads (N = 5 experiments). The efficiency is defined as the number of replication events meeting the selection criteria outlined in molecule selection and processing (Materials and Methods), divided by the average number of correctly tethered beads.

Ensemble leading-strand DNA replication assays.

All reactions contained 25mM Tris-acetate pH 7.5, 5% (v/v) glycerol, 40 µg/ml BSA, 3 mM DTT, 2mM TCEP, 10 mM magnesium acetate, 50 mM potassium glutamate, 0.1 mM EDTA, 5 mM ATP, and 400 µM of each dNTP. The 2.8 kb linear forked templates (1) were primed with a 5'-^{32}P-labeled 37-mer oligonucleotide. Replication assays were performed by first incubating 30 nM CMG with 1.25 nM primed linear forked template in the presence or absence of 60 nM MTC for 5 min at 30ºC, followed by addition of 5 nM RFC, 25 nM PCNA, and 10 nM Pol ε for 4 min in the presence of dATP and dCTP to promote clamp loading and polymerase binding and to prevent the 3'–5' exonuclease activity of Pol ε from removing the primer. Reactions were started by addition of the withheld nucleotides (dGTP and dTTP), 5 mM ATP, and either 600 nM *S. cerevisiae* RPA or 600 nM *E.coli* SSB as indicated. Reactions were allowed to proceed for the indicated times at 30°C and then quenched by adding an equal volume of 2X stop solution (40 mM EDTA and 1% (w/v) SDS). Reactions were run on 1.3% (w/v) alkaline agarose gels at 35 V for 16 h, backed with DE81 paper, and compressed for 12 h. Gels were exposed to a phosphorimager screen and imaged with a Typhoon FLA 9500 (GE Healthcare).

Figure legends Supporting Figures

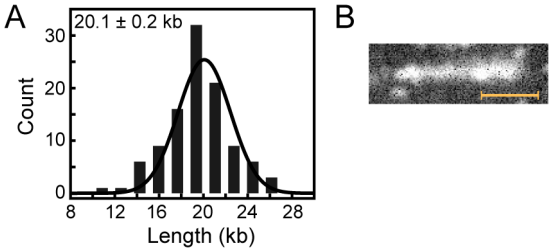

Fig. S1. Length quantification of linear DNA substrate used in tethered bead assay using single-molecule fluorescence imaging. (*A*) Histogram showing the length of linear DNA templates. The black line represents a Gaussian fit to the data with a mean length of 20.1 ± 0.2 kb (*N* = 104 molecules). Error represents standard error of the mean. (*B*) Fluorescence image of a single linear DNA template labeled with SYTOX Orange. Imaging was performed as described in (15) Scale bar represents 10 µm.

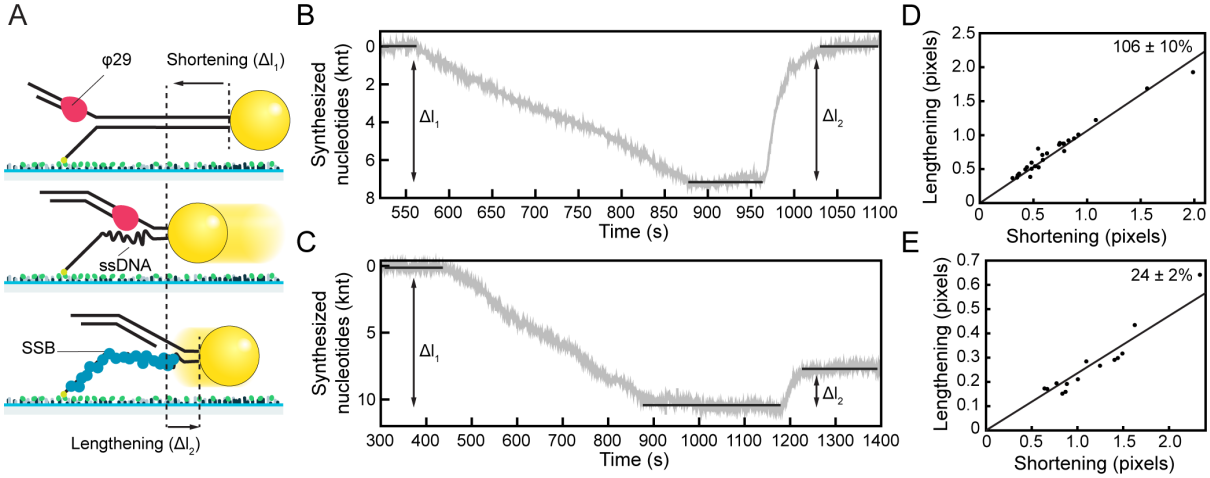

Fig. S2. Determination of conversion factors of ssDNA coated with either RPA or SSB. (*A*) First, leading-strand synthesis shortens (Δl_1) the DNA by converting the lagging-strand DNA to ssDNA. Next, SSB (or RPA) coats the lagging strand resulting in lengthening (Δl_2) of the DNA. In experiments where SSB is present all the time, only an effective shortening is seen, i.e., ($\Delta l_1 - \Delta l_2$). To generate ssDNA, strand-displacement synthesis was performed using 60 U/mL of ϕ29 DNA polymerase (New England Biolabs) on surface-tethered forked DNAs containing replication forks in replication buffer as described (20). After strand-displacement synthesis, the flow cell was washed excessively with replication buffer to remove any residual ϕ29 DNA polymerase. Then either *S. cerevisiae* RPA or *E. coli* SSB was flowed in at 250 nM at 15 µL/min. (*B*) RPA coated ssDNA has a similar length to dsDNA. (*C*) *E. coli* SSB coated ssDNA is shorter than dsDNA. (*D*) Ratio between *S. cerevisiae* RPA lengthening and shortening for 25 DNA molecules. Mean ratio 106 ± 10%. (*E*) Ratio between *E. coli* SSB lengthening and shortening for 14 DNA molecules. Mean ratio 24 ± 2%. Errors represent the error of the fit.

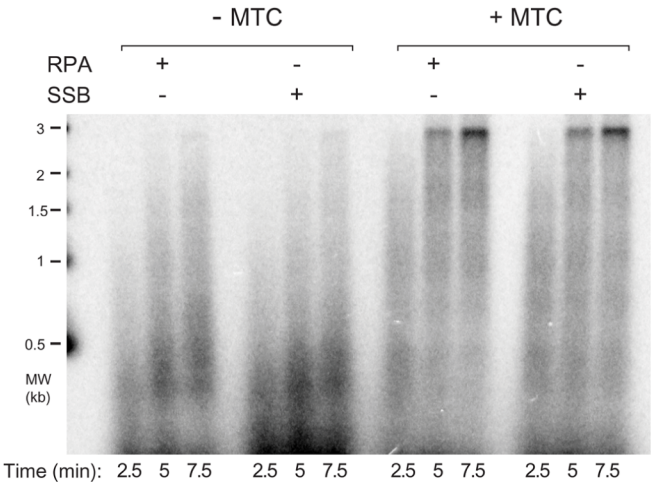

Fig S3. SSB and RPA are interchangeable for leading-strand replication. Alkaline agarose gel of leading-strand products by CMGE leading-strand replisomes Reactions were performed as described in Materials and Methods but included 400 µM dNTPs. Reactions in the presence of either RPA or SSB are shown, both with (lanes 7–12) and without MTC (lanes 1–6). Reactions were stopped at the indicated times.

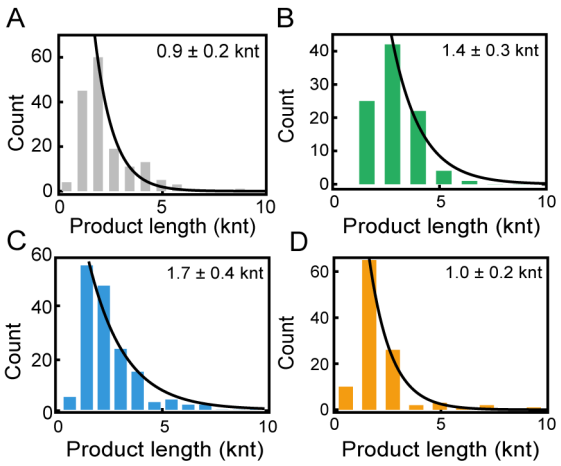

Fig S4. Distributions of product lengths for leading-strand replication. (*A*) Histogram of the total product length per trajectory (0.9 ± 0.2 knt). The fit represents a single-exponential decay function (black line; the first two bins are undersampled and not included in the fit).

The error represents the error of the fit. (*B*) Histogram of the total product length per trajectory for replication by CMGE + Mcm10. A single-exponential fit (black line) shows that the average product length is the same as without Mcm10 (1.4 ± 0.3 knt). (*C*) Histogram of the total product length per trajectory for replication by CMGE + Mcm10 + MTC, fitted to a single-exponential decay function. The total product length (1.7 ± 0.4 knt) is 1.5-fold higher than the value found in (*B*). (*D*) Histogram of the total product length per trajectory using CMGE + Mcm10 + TC, fitted to a single-exponential decay function. The total product length (1.0 ± 0.2 knt) is similar as obtained without TC (*N* = 111 trajectories). In all product-length histograms, the short values are undersampled and not included in the fits.

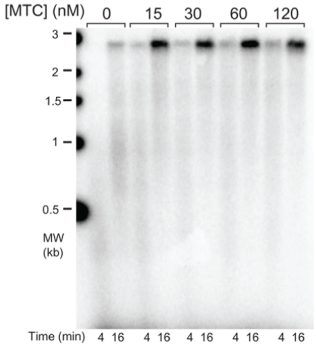

Fig. S5. MTC titration into leading-strand replisome reactions. Alkaline agarose gel of leading-strand products at different concentrations of MTC indicated above the gel. Reactions were stopped at the indicated times below the gel. See Methods for details.

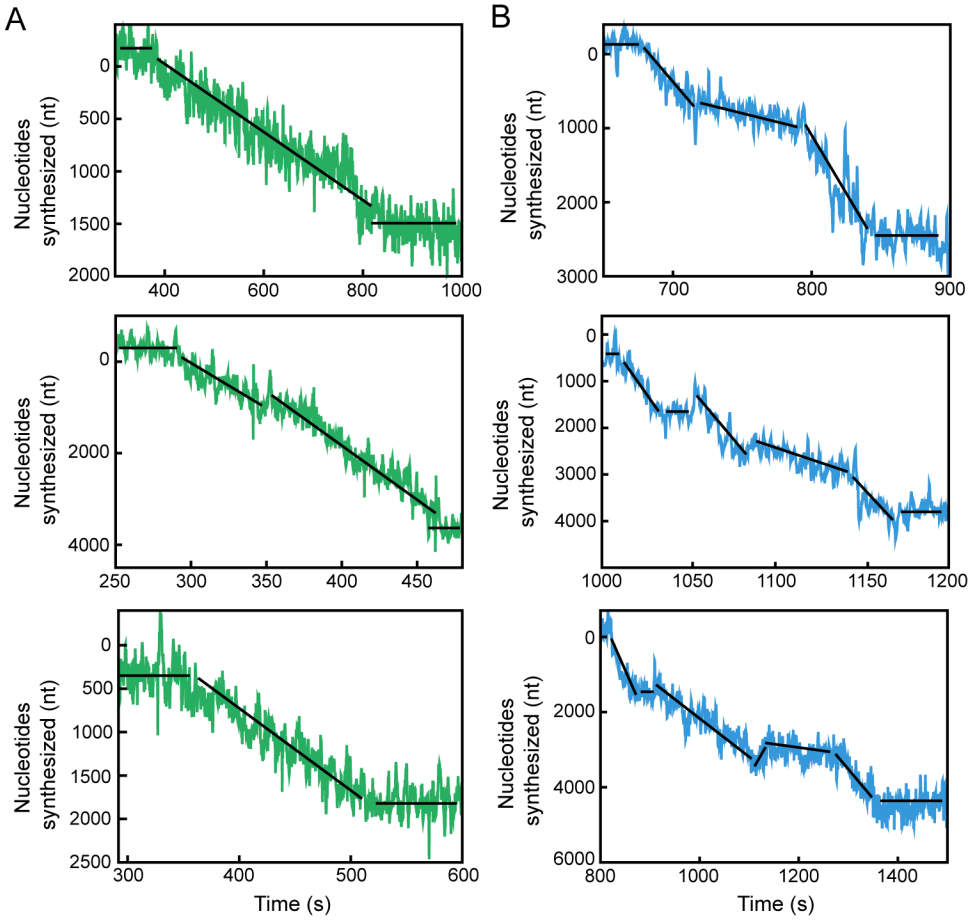

Fig. S6. Six representative trajectories of enzymatic events observed. (*A*) Three example trajectories showing Pol ε-dependent leading-strand synthesis without MTC. (*B*) Three example trajectories showing Pol ε-dependent leading-strand synthesis in the presence of 30 nM MTC. The black lines represent the rate segments identified by the change-point algorithm.

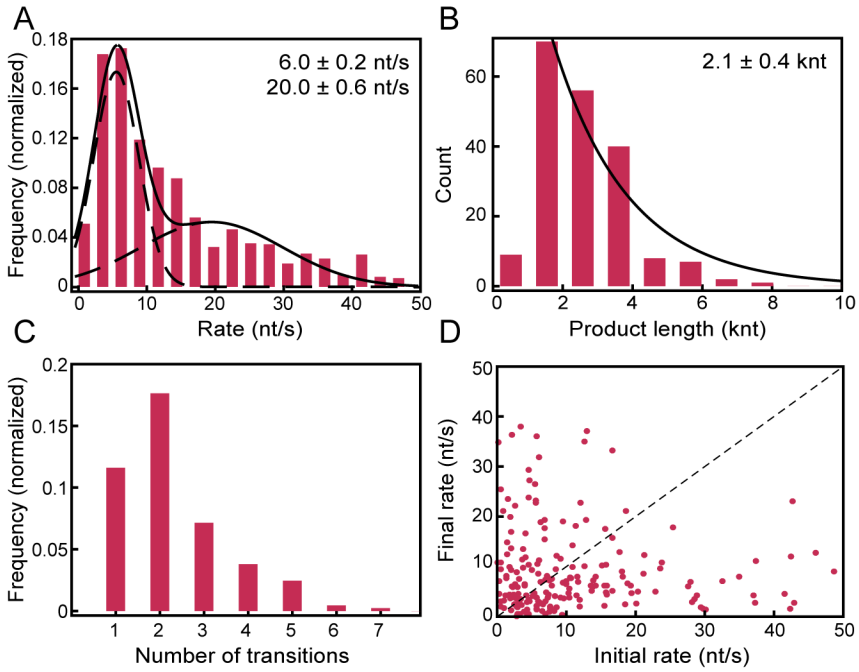

Fig. S7. C-terminally tagged MTC (M_fTC) transiently interacts with the replisome. (*A*) Histogram of the instantaneous single-molecule rates, weighted by segment length for replication by CMGE + Mcm10 + 30 nM M_fTC. The histogram shows a bimodal distribution of the rates. The data were fit with the sum of two Gaussian distributions (black line), resulting in a rate of 6.0 ± 0.2 nt/s for the slow population and 20.0 ± 0.6 nt/s for the fast population (*N* = 195 trajectories). (*B*) Histogram of the total product length per trajectory for replication by CMGE + Mcm10 + 30 nM M_fTC. A single-exponential fit (black line) shows that the total product length is similar to the value measured with MTC (1.7 ± 0.4 knt). (*C*) The number of rate changes per trajectory with M_fTC is similar to MTC (Fig 4). (*D*) Transition plot showing the rate of a segment as a function of the rate of the previous segment for trajectories with multiple segments, with M_fTC present. The distance from the diagonal (dashed line) is (12.1 ± 0.9 nt/s, mean ± s.e.m) similar to MTC (Fig 4).

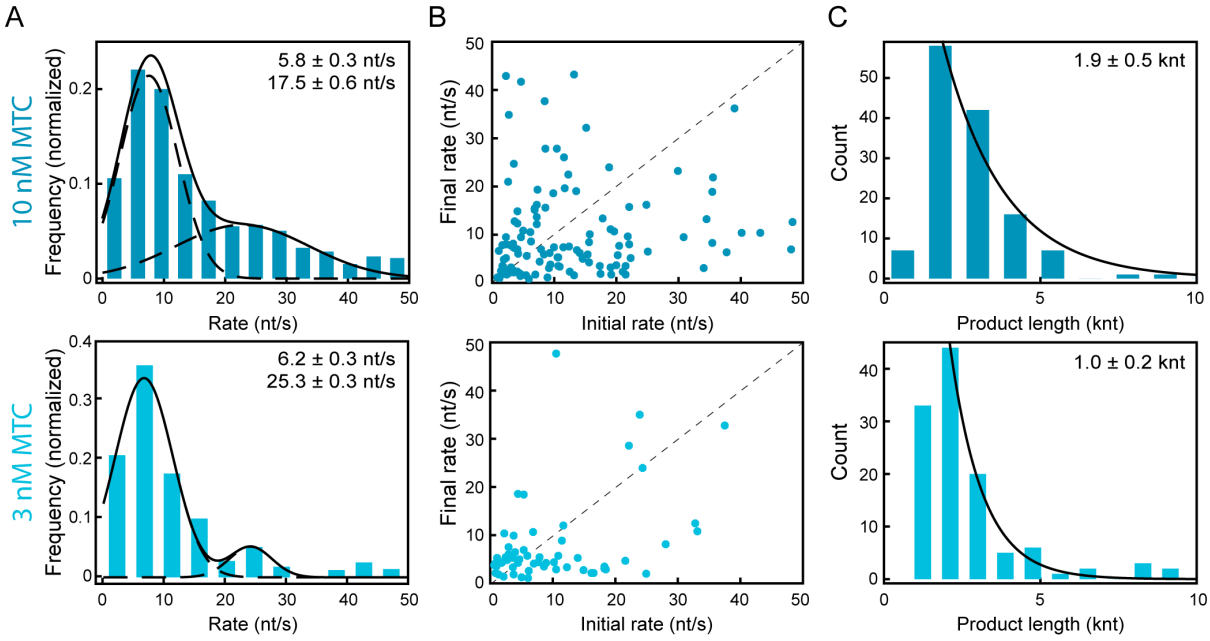

Fig. S8. Lower MTC concentrations result in a reduction in the number of fast rates as well as the frequency of transitions within a single trajectory. (*A*) (Top) Histogram of the instantaneous single-molecule rates, weighted by segment length for replication by CMGE + Mcm10 + 10 nM MTC. The histogram shows a bimodal distribution of the rates. The data were fit with the sum of two Gaussian distributions (black line), resulting in a rate of 5.8 ± 0.3 nt/s for the slow population and 17.5 ± 0.6 nt/s for the fast population (*N* = 251 trajectories). (Bottom) Histogram of the instantaneous single-molecule rates, weighted by segment length for replication by CMGE + Mcm10 + 3 nM MTC. The data were fit with the sum of two Gaussian distributions (black line), resulting in a rate of 6.2 ± 0.3 nt/s for the slow population and 25.3 ± 0.3 nt/s for the fast population (*N* = 184 trajectories). (*B*) Transition plots showing the rate of a segment as a function of the rate of the previous segment for trajectories with multiple segments, with 10 nM (top) and 3 nM (bottom) MTC present. The perpendicular distance from the diagonal (dashed line) is ~2-fold lower when 3 nM MTC is present (4.5 ± 0.7 nt/s, mean ± s.e.m) compared with 10 nM MTC (9.5 ± 0.6 nt/s). (*C*) (Top) Histogram of the total product length per trajectory for replication by CMGE + Mcm10 + 10 nM MTC. A single-exponential fit (black line) shows that the product length is the same as the the value measured with 30 nM MTC (1.9 ± 0.5 knt). (Bottom) Histogram of the total product length per trajectory for replication by CMGE + Mcm10 + 3 nM MTC. A single-exponential fit (black line) shows that the total product length is similar to the value measured without MTC (1.0 ± 0.2 knt).

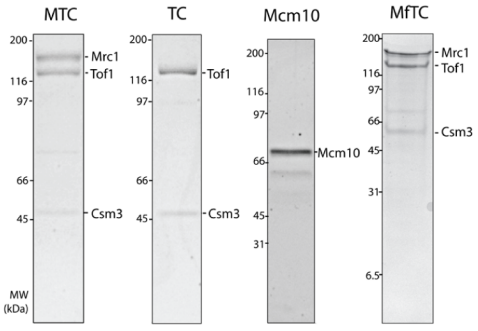

Fig S9. Purification of MTC, TC, Mcm10, and MfTC. Coomassie blue stained SDS-PAGE gels of MTC (left), TC (second from left), Mcm10 (third from left) and MfTC (right panel) are

shown. The three left panels are the protein preparations used for this work, with the exception of Fig. S7, which used the MfTC preparation in the rightmost panel. The left two panels (MTC and TC) are an 8% SDS-PAGE, the third (Mcm10) is a 12% SDS-PAGE, and the last (MfTC) is a 4–20% gradient SDS-PAGE. All proteins contain one or two tags, as documented in Materials and Methods.